Noname manuscript No.
(will be inserted by the editor)

Error propagation dynamics of PIV-based pressure field calculations: What is the worst error?

Zhao Pan · Tadd T. Truscott · Jared P. Whitehead

arXiv:1612.07346v1 [physics.flu-dyn] 21 Dec 2016

Received: date / Accepted: date

Abstract A recent study analyzed the dynamic propagation of error in a PIV-based pressure field calculation by directly analyzing the pressure Poisson equation Pan et al. (2016). We extend these results by quantifying the effect of the spatial dependence of the error profile in the data on the resultant error in the pressure measurement. We design the "worst case error" for the pressure Poisson solver, providing an explicit example where relatively small errors in the experimental data lead to maximal error in the calculated pressure field. This calculation of the worst case error is equivalent to an Euler-Bernoulli beam problem in one-dimension and the Kirchhoff-Love plate problem in two-dimensions, thus connecting the velocity-based pressure calculation, to elastic dynamics. These results can be used to minimize experimental error by avoiding worst case scenarios and to design synthetic velocity errors for future PIV-pressure challenges.

Keywords Pressure calculation · Velocimetry · PIV · Error propagation · Eigenvalue problem · Worst case scenario

Z. Pan
Mechanical and Aerospace Engineering
Utah State University
Logan, UT 84322, USA
E-mail: panzhao0417@gmail.com

T. T. Truscott
Mechanical and Aerospace Engineering
Utah State University
Logan, UT, 84322, USA
E-mail: taddtruscott@gmail.com

J. P. Whitehead
Mathematics Department
Brigham Young University
Provo, UT 84602, USA
E-mail: whitehead@mathematics.byu.edu

1 Introduction

Velocity is the most pervasive measurement fluid-experimentalists use to gather information about flow fields. Various techniques over the past 20 years have supplied the fluids community with improved spatial and time resolved experimental data including: hot-wire anemometry, Laser Doppler Velocimetry (LDV), and Particle Image Velocimetry (PIV)) Adrian (2005); Westerweel et al. (2013). Today's state-of-the-art systems can provide high-resolution volumetric velocity field data that can even compete with modern numerical methods Moin et al. (1998). Velocity measurements are also fundamentally important to a wide range of industrial, military, medical and natural flow problems such as those associated with aircraft wings, shockwave interactions and vortex formation in prosthetic heart valves.

Although most techniques for non-invasive measurements have focused on the velocity field, extension to the pressure field has many promising aspects Van Oudheusden (2013). Uncertainty quantification for the velocity field from such techniques is well-studied, but most modern experiments do not assess uncertainties in the pressure estimates and thus do not translate uncertainties in the velocity field measurements to the pressure field calculation.

In an effort to clarify this issue, Charonko et al. (2010) benchmarked various PIV-based pressure calculation methods with numerical and physical experiments. They reported that the performance of the PIV-based pressure calculation is sensitive to many factors. Not surprisingly they noted that several conditions (temporal and spatial resolution, velocity error, smoothing techniques, pressure solver scheme, flow type, etc.) impact the error propagation. In this pioneering research, they indicate that there is no universal or optimal method to reduce errors in the pressure calculation but that such reductions are case dependent. They did not report specifically on the effect of the error profile in the velocimetry measurements on the resultant error in the calculated pressure field.

De Kat and Van Oudheusden (2012) commented that the central finite difference based Poisson solver acts as a low-pass filter, effectively eliminating the high-frequency errors in the pressure calculation. The ratio of the grid spacing of the numerical method to the temporal or spatial wave length of the experimental data impacts the frequency response of the pressure Poisson solver. Specifically, high frequency data is filtered resulting in the loss of high-frequency physics. Similarly, low frequency errors are more likely to propagate through the pressure calculation. For example, a high Reynolds number turbulent flow field (high-frequency physics) with a calibration error in PIV (low frequency error) would result in large amount of error propagated to the pressure field. Their study provided the first analysis on the error associated with frequency, however, the results are limited to the scale of the numerical scheme.

In a recent study, Pan et al. (2016) reported that the profile of the error field in the data (ϵ_f) affects the error propagation (e.g., differences between peak-locking, calibration error, and random error, etc.). Their results qualitatively

unravel the coupled effects of the error and velocity profiles on the pressure calculation. They quantify how the error levels in the pressure field calculation ($||\epsilon_p||_{L^2(\Omega)}$) can be bounded by the error in the data ($||\epsilon_f||_{L^2(\Omega)}$, $||\epsilon_h||_{L^\infty(\partial\Omega)}$) and some Poincare constant(s) (C_D) which relate to the dimension and geometry of the domain (e.g., $||\epsilon_p||_{L^2(\Omega)} \leq C_D||\epsilon_f||_{L^2(\Omega)} + ||\epsilon_h||_{L^\infty(\partial\Omega)}$, for the Dirichlet case). This recent work does not identify a worst case error profile, or establish an error profile that will saturate the upper bound on the error in the calculated pressure field.

Here, we present a systematic methodology for finding the "worst case error profile" (called "worst error" hereafter) for the velocity-based pressure calculation. This provides a surprising connection between the fluid mechanics and elastic dynamics communities. The final calculation of the worst error is equivalent to an Euler-Bernoulli beam problem in one-dimension and the Kirchhoff-Love plate problem in two-dimensions. From a practical perspective, these results can be used to i) minimize experimental error by avoiding worst case scenarios and ii) used to design worst case benchmarking challenges for pressure solvers.

In this paper, first we *define* the worst error possible for the velocity-based pressure calculation in Sec. 2, then we *calculate* the worst error in Sec. 3 and appendix A. Two illustrative examples (one dimensional and two dimensional cases) are given in Sec. 4 followed by a proposed protocol for experimentalists and a summary in Sec. 5.

2 Problem statement

The propagation of error in the PIV-based pressure calculation can be modeled via Poisson's equation

$$\epsilon_f = \nabla^2 \epsilon_p, \tag{1}$$

where ϵ_f and ϵ_p are the error in the data field and calculated pressure field, respectively Pan et al. (2016). The error level is measured by the L^2 norm, for example the error level of the calculated pressure field is

$$||\epsilon_p||_{L^2(\Omega)} = \sqrt{\frac{\int \epsilon_p^2 d\Omega}{|\Omega|}}, \tag{2}$$

where Ω is the domain of the flow field, and $|\Omega|$ is the length, area or volume of the domain, depending on the dimension. This L^2 norm is intuitively a measurement of the space-averaged power of the error. The goal is to determine the error profiles in the data field (ϵ_f) that lead to the worst error (measured by this norm) in the calculated pressure field (ϵ_p) relative to the error in the data itself. Thus finding the worst error can be defined as a variational problem with ϵ_f as the desired function, i.e., we seek ϵ_f to satisfy:

$$\max_{\epsilon_f} Ar = \max_{\epsilon_f} \frac{||\epsilon_p||_{L^2(\Omega)}}{||\epsilon_f||_{L^2(\Omega)}}, \tag{3}$$

subject to (1) with the appropriate boundary conditions on the domain. The ratio Ar is the ratio of the error from the PIV-based pressure calculation relative to the error from the input data. It is an error amplification ratio if the PIV-based pressure calculation is considered a single-input single-output dynamical system. We are only interested in the situations where the denominator is non-zero as this indicates that the power in the error in the data is nonzero, thus avoiding the mathematical singularity in Ar.

3 Calculation of the worst error

Here we consider the maximization problem of (3) with Dirichlet boundary conditions on the data ϵ_f (Neumann and mixed boundary conditions can be treated similarly). Using the Poisson equation we can simplify Ar to be in terms of the output error only:

$$\max_{\epsilon_p} \frac{||\epsilon_p||_{L^2(\Omega)}}{||\nabla^2 \epsilon_p||_{L^2(\Omega)}}, \quad \epsilon_p = g \text{ for } x \in \partial\Omega, \tag{4}$$

where g is a sufficiently smooth function that specifies the boundary condition. This can be reformulated using a constant Lagrange multiplier with the constraint that the denominator is normalized (see Gelfand and Fomin (1991) for example). In other words, we seek the solution of:

$$\begin{aligned} &\max_{\epsilon_p} \quad J[\epsilon_p] = \max_{\epsilon_p} \int_\Omega \left\{ |\epsilon_p|^2 + \lambda |\nabla^2 \epsilon_p|^2 \right\} dx, \\ &\text{s.t.} \qquad \int_\Omega |\nabla^2 \epsilon_p|^2 dx = 1, \quad \text{and} \quad \epsilon_p = g \text{ for } x \in \partial\Omega. \end{aligned} \tag{5}$$

Standard application of the Calculus of variations (see Gelfand and Fomin (1991)) then indicates that the maximizer for this problem must satisfy the Euler-Lagrange equations:

$$\nabla^4 \epsilon_p = -\frac{1}{\lambda} \epsilon_p, \tag{6}$$

with $\epsilon_p = g$ and $\nabla^2 \epsilon_p = 0$ on $\partial\Omega$, subject to $|\Omega| \|\nabla^2 \epsilon_p\|^2_{L^2(\Omega)} = 1$.

The additional boundary condition $\nabla^2 \epsilon_p = 0$ is the 'natural' boundary condition that arises because the variational formulation is quadratic in the second derivatives of ϵ_p, and we have specified only the first order Dirichlet condition from physical considerations. As indicated above, other boundary conditions (other than Dirichlet) will result in a different type of natural boundary condition as listed in table 1 (see Gelfand and Fomin (1991)).

Equation (6) is the same as the eigenvalue problem that arises as the characteristic equation of transverse vibration of beams or plates Timoshenko et al. (1937). Thus as long as the boundary conditions are prescribed carefully (as they are for the Dirichlet case studied here) we are guaranteed that there is a countable number of solutions to this system with corresponding eigenvalues

Table 1 Type of boundary conditions (BCs) of the original pressure Poisson equation and the corresponding BCs of the eigenvalue problem of the worst error and the induced natural boundaries. G, g, H, and h are functions on the boundary $\partial\Omega$, and $\hat{n}$ is the unit outward pointing normal on $\partial\Omega$.

Type of BCs	BC of pressure Poisson eq.	Essential BC of eigenvalue problem	Natural BC of eigenvalue
Dirichlet	$p = G$	$\epsilon_p = g$	$\nabla^2\epsilon_p = 0$
Neumann	$\nabla p \cdot \hat{n} = H$	$\nabla\epsilon_p \cdot \hat{n} = h$	$\nabla\left(\nabla^2\epsilon_p\right) \cdot \hat{n} = 0$

$\mu_k = -\frac{1}{\lambda_k} > 0$. The smallest of these eigenvalues μ_1 and corresponding eigenfunction yield the maximal field for Ar. Thus the worst error profile is indeed determined by the fundamental features of the flow domain (i.e., dimension, size and shape of the domain, and the type of boundary conditions), see also Pan et al. (2016)).

This fourth order variational problem is studied in great detail in elastic mechanics (e.g., Landau and Lifshitz (1986), Timoshenko et al. (1937)). Specifically, it is equivalent to the Euler-Bernoulli beam problem in 1D, and the Kirchhoff-Love plates problem in 2D. Solutions with standard boundary conditions and in basic domains are tabulated in text books (e.g. Morse et al. (1948), Harris and Piersol (2002)).

4 Examples

We consider two idealized problems that illustrate the relative effects of error in the data for a variety of different error profiles as compared to the optimal error profile that yields the maximal error in the calculated pressure field. First, we use a 1D example to demonstrate the relative effects of error profiles distinctly different from the maximal one. Second, a more realistic 2D example is detailed, showing how to use the worst error in the data field to calculate the worst error in the velocity field.

4.1 1D example

Consider the flow profile along the center line of a steady Poiseuille flow ($x \in [0, 1]$) driven by a pressure gradient ($dp/dx = -1$), whose velocity profile is defined as $u = 1$. The corresponding PIV-based pressure calculation problem is governed by an ordinary differential equation (ODE) based on the Poisson approach (e.g. De Kat and Van Oudheusden (2012)), $d^2p/dx^2 = 0$, with Dirichlet boundary conditions $p(0) = 1$, and $p(1) = 0$. The exact solution of the pressure profile should be $p = 1 - x$. To see how different error profiles in the data influence the solution, we consider several different ϵ_f all with constant power ($||\epsilon_f||_{L^2(\Omega)} = 1$) as shown in (Fig. 1(a)). Solving the error contaminated PIV-pressure problem ($d^2\tilde{p}/dx^2 = \epsilon_f$, where $\tilde{p} = p+\epsilon_p$), we compare the calculated pressure field ($\tilde{p}$) with the exact pressure field (Fig. 1(b)).

Table 2 Analogy between the beam vibration problem and the worst error problem raised by the PIV-based pressure calculation. (a) The governing equations are normalized to expose the mathematical roots shared by the two problems. $Y(x,t) = X(x)T(t)$ is the deflection of the beam, which is a function of $x \in [0, L]$, and time $t \in [0, \infty)$. $(\cdot)'$ indicates the derivative with respect to x, and $(\ddot{\cdot})$ indicates the time derivative. (b) The derivations for the characteristic equations can be found in Timoshenko et al. (1937) (for the beam problem) and in Sec.3 (for the PIV-pressure error problem). (c) k and λ are constants of the characteristic equations, but they are all related to the natural frequencies of the system (e.g. ω is the natural frequency of the beam). (d) The same BCs are enforced as a simple example for both problems: a simply supported beam or a Dirichlet boundary condition with no error from the measurement ($\epsilon_f = 0$ on $\partial\Omega$).

Physical interpretation	Beam vibration problem	Velocity-pressure error problem
Governing eq.[(a)]	$Y'''' = -\ddot{Y}$	$\nabla^2\epsilon_p = \epsilon_f$
Characteristic eq.[(b)]	$X'''' = k^4 X$	$\nabla^4\epsilon_p = -\lambda^{-1}\epsilon_p$
Normal modes	X(Beam deflection)	ϵ_p(Error in pressure calculation)
Natural frequencies[(c)]	$k = \omega^{-1/2}$	λ (Lagrange multiplier, $\lambda < 0$)
Boundary conditions[(d)]	$X(0) = X(L) = 0$	$\epsilon_p(0) = \epsilon_p(L) = 0$
	$X''(0) = X''(L) = 0$	$\epsilon_p''(0) = \epsilon_p''(L) = 0$

We can see that both the profile and power of the error in the calculated pressure field ($\epsilon_p = \tilde{p} - p$) highly depend on the profile of the error in the data (Fig. 1(c)).

In this 1D example, the worst error can be found by solving the fourth order eigenvalue problem:

$$\frac{d^4\epsilon_p}{dx^4} = -\frac{1}{\lambda}\epsilon_p, \tag{7}$$

where λ is the Lagrange multiplier, which physically relates to the natural frequencies of the flow field (See Appendix (A.1) for details). The worst error in the data corresponds to the first eigenvalue with eigenfunction $\epsilon_f = \sqrt{2}\sin\pi x$, yielding the largest error in the pressure calculation relative to the power of the error in the data (Fig 1(a)). Notice equation (7) is the characteristic equation of an Euler-Bernoulli beam, which determines the principle modes of prismatical beams under lateral vibration. For the specified boundary conditions ($\epsilon_f(0) = \epsilon_f(1) = 0$), the worst error problem raised by the velocity-pressure calculation is similar to a beam that is simply supported on each end (see Table 2).

Figure 1 illustrates 4 different enforced error profiles, where ϵ_{f1} is the computed maximal error (Fig 1(a)) inducing profile (Fig 1(c)). For example, the high frequency error profile in the data given by ϵ_{f3} has the same amplitude as ϵ_{f1} ($\max|\epsilon_{f1}| = \max|\epsilon_{f3}| = \sqrt{2}$), and the power is also the same ($||\epsilon_{f1}||_{L^2(\Omega)} = ||\epsilon_{f3}||_{L^2(\Omega)} = 1$). However, the induced error in the pressure calculation ($||\epsilon_{p3}||_{L^2(\Omega)} = 0.014$) is significantly less than the worst case ($||\epsilon_{p1}||_{L^2(\Omega)} = 0.101$). This implies that high frequency errors (e.g., peak-locking could be one of the typical sources) affect the error propagation less than the low frequency errors. ϵ_{f4} has as a sharp tall peak which may be indicative of a local error such as spurious vectors. This error is concentrated on a small spatial scale and is smoothed out by the Poisson operator (not necessarily

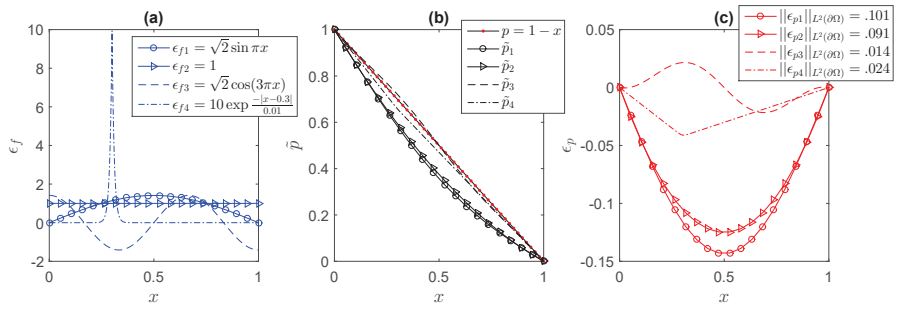

Fig. 1 (a) Profiles of error in the data (ϵ_f). Expressions are shown in the legend. (b) Calculated pressure profile ($\tilde{p}$) from contaminated pressure equation, compared with the true value (p). (c) Error profile in the pressure calculation (ϵ_p). The error level ($||\epsilon_p||_{L^2(\Omega)}$) in the calculated pressure field are listed in the legend.

reliant on the numerical scheme as reported by De Kat and Van Oudheusden (2012)) so that ϵ_{p4} is significantly less than the maximal error. In contrast, global low amplitude errors such as ϵ_{f2} (e.g., could be due to calibration) can yield relatively large error in the pressure calculation (ϵ_{p2}). This example gives a possible reason why low-pass filters of the PIV post-processing do not improve PIV-based pressure solvers (reported observation of Charonko et al. (2010)).

The error level in the data is constrained to unity ($||\epsilon_{fi}||_{L^2(\Omega)} = 1$) hence, the error amplification ratio Ar is numerically equal to the error level in the calculated pressure ($||\epsilon_{pi}||_{L^2(\Omega)}$) as shown in the legend of Fig. 1(c). Note that this example indicates that the total error can vary by an order of magnitude even when the error in the data is normalized. This 1D example confirms that the error profile in the data significantly affects the error in the calculated pressure field. The result confirms the findings by Pan et al. (2016); Charonko et al. (2010), and extends the work of De Kat and Van Oudheusden (2012).

4.2 2D example

We also provide a 2D example with small error introduced. We consider a vortex in a 1×1 domain in Cartesian coordinates. The velocity field is $u = -y$, $y \in [0, 1]$; $v = x$, $x \in [0, 1]$, where u and v are the two components of the velocity field $\boldsymbol{u}$ in the x and y direction, respectively. The corresponding data of the pressure Poisson equation is $f = \nabla \cdot (\boldsymbol{u} \cdot \nabla)\boldsymbol{u} = -2$. Thus the pressure field is $p = (x^2 + y^2 - x - y + 0.5)/2$. The Dirichlet boundary conditions are defined as $p = (y^2 - y + 0.5)/2$ for $x = 0$ or 1, and $p = (x^2 - y + 0.5)/2$ for $y = 0$ or 1. The worst error is calculated as $\epsilon_f = -\sin(\pi x)\sin(\pi y)/2$ to the data with a small power ($||\epsilon_f||_{L^2(\Omega)} = \delta = 1/4$ as in Fig. 2(a)). We calculate the error contaminated pressure field $\tilde{p}$ (Fig. 2(b)) with a numerical Poisson solver (see Reimer and Cheviakov (2013)), and find the error in the pressure filed ϵ_p with power $||\epsilon_p||_{L^2(\Omega)} \approx 0.0127$ (see Fig. 2(c)), which may seem to be a modest

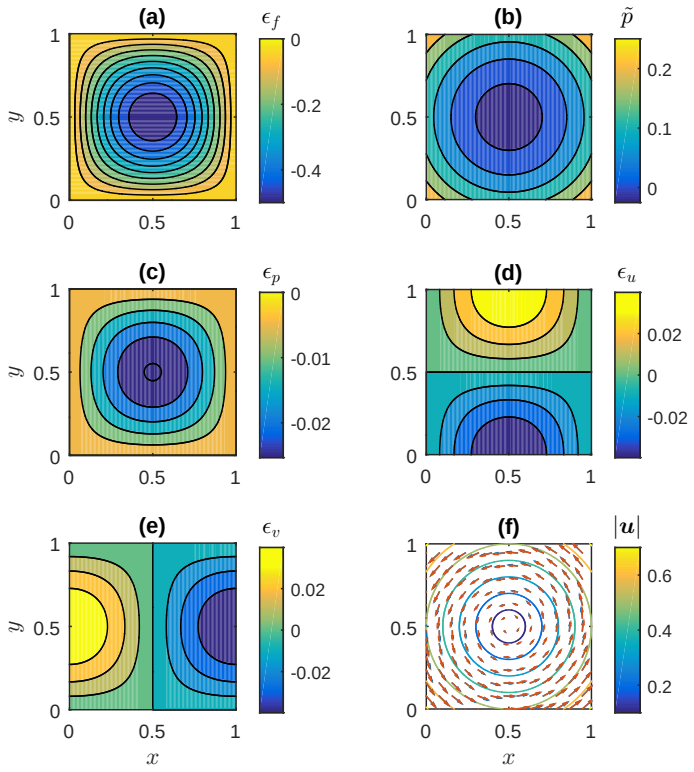

Fig. 2 The 2D vortex example. (a) Error in the data field. (b) Error contaminated pressure calculation. (c) Error in the calculated pressure field. (d & e) Error in the velocity field, x and y component, respectively. (f) Quiver plot of the velocity field ($\boldsymbol{u}$, blue) and the error contaminated velocity field ($\tilde{\boldsymbol{u}}$, red) overlap on the contour of velocity magnitude ($|\boldsymbol{u}|$). The grid of the quiver plot is 10 times coarser than the original one used in simulation for better visualization.

amplification ratio. However, it is more than 10% relative error if we compare the error with the true value of the pressure field ($||\epsilon_p||_{L^2(\Omega)}/||p||_{L^2(\Omega)} \approx 12.8\%$).

Additionally, we can identify errors in the velocity field ($\epsilon_{\boldsymbol{u}}$) that yield the worst error in the data by noting that:

$$\epsilon_f \approx -2\left(\frac{\partial u}{\partial x}\frac{\partial \epsilon_u}{\partial x} + \frac{\partial v}{\partial x}\frac{\partial \epsilon_u}{\partial y} + \frac{\partial u}{\partial y}\frac{\partial \epsilon_v}{\partial x} + \frac{\partial v}{\partial y}\frac{\partial \epsilon_v}{\partial y}\right) \tag{8}$$

(see Pan et al. (2016) for more details). Substituting the velocity field and worst error in the data field into (8), we can find the coresponding worst error in the velocity field. In this example, one solution to (8) is shown in figure 2(d) and (e) where the two components of the worst error in the ve-

locity field are $\epsilon_u = \sin(\pi x)\cos(\pi y)/8\pi$ and $\epsilon_v = -\cos(\pi x)\sin(\pi y)/8\pi$, respectively (see appendix B for more details). Figure 2(f) shows quiver plots of the true value of the velocity field (e.g., $\boldsymbol{u}$, blue arrows) and an error contaminated velocity field ($\tilde{\boldsymbol{u}}$, red arrows) and the overlap on the contour of the velocity ($|\boldsymbol{u}| = \sqrt{u^2 + v^2}$). The two velocity fields are almost identical (e.g., $\max|\epsilon_{\boldsymbol{u}}|/\max|\boldsymbol{u}| \approx 5.6\%$), yet relatively large errors appear in the calculated pressure field ($\max|\epsilon_p|/\max|p| \approx 10.1\%$, see Fig. 2(c)).

Replacing the unknown true value of the velocity field ($\boldsymbol{u}$) with the error contaminated velocity field ($\tilde{\boldsymbol{u}}$, which would be obtained directly from PIV measurements), we have

$$\epsilon_f \approx -2\left(\frac{\partial\tilde{u}}{\partial x}\frac{\partial\epsilon_u}{\partial x} + \frac{\partial\tilde{v}}{\partial x}\frac{\partial\epsilon_u}{\partial y} + \frac{\partial\tilde{u}}{\partial y}\frac{\partial\epsilon_v}{\partial x} + \frac{\partial\tilde{v}}{\partial y}\frac{\partial\epsilon_v}{\partial y}\right) \tag{9}$$

which holds when the error is small. Solution of this equation gives an approximation of the error that occurs in the velocity field, given the measured velocity.

4.3 Protocol for experimentalists

To summarize this analysis, we describe a work flow for experimental design. The practical question is what the worst possible error in pressure can be given a known velocity field (i.e., measured velocity includes error), and what type of error in the measured velocity field will produce such error in the pressure. First, based on the fundamental features of the flow domain (e.g., dimension and boundary conditions of the domain, etc.) the calculation in Sec. 3 gives the worst error in the data ϵ_f (e.g., Fig 2(a)). Second, substituting the worst error in the data field ϵ_f into (1) and the solution of the error Poisson equation gives the worst possible error in the pressure calculation, which can be considered an *a prior* error estimation of the calculated pressure. This estimation is different than Azijli et al. (2016), relying on the dynamics of the Poisson operator rather than a statistics-based posterior estimation

Since the experimentalist would typically measure the velocity field $\tilde{\boldsymbol{u}}$ (e.g., the red vector field in Fig 2(f)), they can use the calculated ϵ_f and measured velocity field $\tilde{\boldsymbol{u}}$ from velocimetry techniques, to solve (9) to find the worst error estimate in the velocity field $\epsilon_{\boldsymbol{u}}$ (e.g., Fig 2(d, e)). This estimate informs the practitioner of what errors in the velocity field are amplified by the pressure solver. Knowing the worst error profile in the velocity field ($\epsilon_{\boldsymbol{u}}$) can help engineers to avoid error profiles similar to ($\epsilon_{\boldsymbol{u}}$) by striving to minimize the most unfriendly error areas in the velocity profile. For example, in the 2D example, experimentalists would avoid systematic errors that are 'positive' on one side of the domain and 'negative' on the other (e.g., notice the hill at the top and basin at the bottom of Fig. 2(d)). A skewed calibration could introduce errors similar to these, and experimentalists should pay careful attention to avoid them especially in this particular example. In addition, the worst error in the velocity field ($\epsilon_{\boldsymbol{u}}$) can be used as a benchmark for the most challenging

test cases for PIV-based pressure calculation scheme development (e.g., the NIOPLEX project).

At last, we emphasize that i) The worst error discussed in this paper is the worst case scenario, and thus may not necessarily happen in real experimental practice, and is most useful as a relevant upper bound. ii) The profile of the worst error varies based on both the fundamental features (type of boundary conditions, dimension and shape of the domain, etc.) of a particular flow domain and the particular velocity profile of the flow. Thus, the error propagation dynamics of a velocimetry based pressure calculation is indeed complicated and 'flow-dependent' and there is no 'optimal' universal experimental setting for all types of flow (see also Charonko et al. (2010)). Hence, the experimentalist should apply analysis like the one presented here to each new flow situation. iii) The worst error in the velocity field is not unique. Indicating that there are several potential velocity profiles that may exhibit the worst propagation of error into the pressure field calculation.

5 Conclusions

We have presented the worst case error in a data field for a velocity-based pressure calculation by solving a corresponding variational problem. The derivation of the worst error surprisingly leads to connections in the well established beam or plate vibration theory from elastic mechanics. The solution gives both an error estimate for the worst error pressure and indicates how that pressure field error is connected to the velocity error. It gives the experimentalist insight into where the errors in the pressure field are most affected by errors in the velocity field. This can be a helpful aid in determining which errors in the velocity can impact the pressure calculation the most. Finally, the worst error can be used to make the most challenging test cases for PIV-based pressure reconstruction algorithms.

Acknowledgements

We would like to thank Dr. Jesse Belden for practical discussions. ZP would like to thank Dr. Wenyan Jiang for financial support.

A Worst error in the data field (ϵ_f) calculation examples

A.1 The one-dimensional example

To illustrate the maximal possible error ratio, we will calculate the 1D case as an example with $g = 0$ on $x \in [0, 1]$. Equation (6) becomes (7): $\epsilon_p^{''''} = -\lambda^{-1}\epsilon_p$, with boundary conditions $\epsilon_p(0) = \epsilon_p(1) = \epsilon_p(0) = \epsilon_p(0)^{''} = \epsilon_p(1) = \epsilon_p(1)^{''} = 0$. The general solution is

$$\epsilon_p(x) = C_1 \cos\beta x + C_2 \sin\beta x + C_3 \cosh\beta x + C_4 \sinh\beta x,$$

where C_i $(i = 1 \dots 4)$ are constants to be determined, and $\beta = \sqrt[4]{-\lambda^{-1}}$. Applying the boundary conditions, and the normalization condition $\|\epsilon_f(x)\|_{L^2(\Omega)} = 1$, we find that the solution is given by $\epsilon_p(x) = \pm\sqrt{2}/(k^2\pi^2)\sin(k\pi x)$. The maximum of Ar occurs for $k = 1$ wherein the maximal error is induced by the error in the data, $\epsilon_f(x) = \pm\sqrt{2}\sin(\pi x)$ with corresponding error in the calculated pressure profile $\epsilon_p(x) = \pm\sqrt{2}/\pi^2\sin(\pi x)$ so that the error amplification ratio is $Ar = \pi^{-2} \approx 0.101$.

A.2 The two-dimensional example

Similar to the 1D case, with boundary conditions $\epsilon_p(x, y) = \nabla^2\epsilon_p(x, y) = 0$, on $\partial\Omega$, the solution to (6) is

$$\epsilon_p(x, y) = C\sin(m\pi x)\sin(n\pi y), \tag{10}$$

where C is a constant, and $m, n = 1, 2, \dots$. With the constraint that $\|\nabla^2\epsilon_p\|_{L^2(\Omega)} = \delta$, we determine the constant $C = \pm 2\delta/(m^2+n^2)\pi^2$. When $\delta = 1/4$ as in the main body of this article, $m = n = 1$ leads to the worst error in the data given by: $\epsilon_f(x, y) = \pm\sin(\pi x)\sin(\pi y)/2$, and gives maximal relative error $Ar = 1/2\pi^2$.

B Worst error in the velocity field (ϵ_u) calculation

Substituting the velocity profile and the worst error in the data field to (8) leads to

$$-2\frac{\partial\epsilon_u}{\partial y} + 2\frac{\partial\epsilon_v}{\partial x} = \pm\frac{1}{2}\sin(\pi x)\sin(\pi y). \tag{11}$$

One of the solutions to (11) can be obtained by solving

$$-2\kappa_1\frac{\partial\epsilon_u}{\partial y} = 2\kappa_2\frac{\partial\epsilon_v}{\partial x} = -\frac{1}{4}\sin(\pi x)\sin(\pi y), \tag{12}$$

where $\kappa_1^{-1} + \kappa_2^{-1} = 2$, with certain boundary condition such as $\bar{\epsilon}_{\boldsymbol{u}} = \int \epsilon_{\boldsymbol{u}} d\Omega = \xi$, and an auxiliary condition such as $\kappa_1/\kappa_2 = \zeta$. This solution describes the two components of the worst error in the velocity field as $\epsilon_u = \sin(\pi x)\cos(\pi y)/8\pi$ and $\epsilon_v = -\cos(\pi x)\sin(\pi y)/8\pi$, respectively. In this particular example, $\xi = 0$ means that we assume the error in the velocity field is mean zero; and $\zeta = 1$ implies that the error on the x and y components contributes to the error in the data equally.

It is worth noting that specifying velocity fields u and v in (8) may not yield a unique error field ϵ_u and ϵ_v. To do so, we would need to supplement (8) with boundary conditions, and auxiliary conditions. In particular instances where the experimental setup can dictate such conditions, they should be used, but the reader is cautioned that such auxiliary conditions are applied to the error fields, not the velocity field. Thus in a generic setting, the worst error is realized in the velocity field by several potential error fields, each of which may have a different physical interpretation.

References

R.J. Adrian, Twenty years of particle image velocimetry. Experiments in fluids **39**(2), 159–169 (2005)

I. Azijli, A. Sciacchitano, D. Ragni, A. Palha, R.P. Dwight, A posteriori uncertainty quantification of PIV-based pressure data. Experiments in Fluids **57**(5), 1–15 (2016)

J.J. Charonko, C.V. King, B.L. Smith, P.P. Vlachos, Assessment of pressure field calculations from particle image velocimetry measurements. Measurement Science and Technology **21**(10), 105401 (2010)

R. De Kat, B. Van Oudheusden, Instantaneous planar pressure determination from PIV in turbulent flow. Experiments in fluids **52**(5), 1089–1106 (2012)
I.M. Gelfand, S.V. Fomin, *Calculus of Variations* (Dover, ???, 1991)
C.M. Harris, A.G. Piersol, *Harris' shock and vibration handbook*, vol. 5 (McGraw-Hill New York, ???, 2002)
L.D. Landau, E.M. Lifshitz, Course of theoretical physics, theory of elasticity (1986)
P. Moin, , K. Mahesh, Direct numerical simulation: A tool in turbulence research. Annual Review of Fluid Mechanics **30**(1), 539–578 (1998). doi:10.1146/annurev.fluid.30.1.539. http://dx.doi.org/10.1146/annurev.fluid.30.1.539
P.M. Morse, A.S. of America, A.I. of Physics, *Vibration and sound*, vol. 2 (McGraw-Hill New York, ???, 1948)
Z. Pan, J. Whitehead, S. Thomson, T. Truscott, Error propagation dynamics of piv-based pressure field calculations: How well does the pressure poisson solver perform inherently? Measurement Science and Technology **27**(8), 084012 (2016). http://stacks.iop.org/0957-0233/27/i=8/a=084012
A.S. Reimer, A.F. Cheviakov, A matlab-based finite-difference solver for the poisson problem with mixed dirichlet–neumann boundary conditions. Computer Physics Communications **184**(3), 783–798 (2013)
S. Timoshenko, et al., Vibration problems in engineering, Technical report, 1937
B. Van Oudheusden, PIV-based pressure measurement. Measurement Science and Technology **24**(3), 032001 (2013)
J. Westerweel, G.E. Elsinga, R.J. Adrian, Particle image velocimetry for complex and turbulent flows. Annual Review of Fluid Mechanics **45**(1), 409–436 (2013)